SH41D-2398

Interstellar Flow Longitude from Pickup Ion Cut-off Observations at 1 AU

E. Möbius[1], M.A. Lee[1], G. Gloeckler[2], C. Drews[3]

[1]Space Science Center & Department of Physics, University of New Hampshire, Durham, NH 03824

[2] Department of Atmospheric, Oceanic, & Space Sciences, University of Michigan, Ann Arbor, MI, U.S.A.

[3]Institut für Experimentelle und Angewandte Physik, Christian-Albrecht-Universität, Kiel, Germany

e-mail: eberhard.moebius@unh.edu

Supported by:
NASA and DLR

Introduction

The Interstellar Boundary Explorer (IBEX) obtains a very precise relation between the interstellar neutral (ISN) flow longitude $\lambda_{ISN\infty}$ and speed $V_{ISN\infty}$, with substantially larger uncertainty separately for $\lambda_{ISN\infty}$, which defines a parameter tube that connects ISN longitude, latitude, speed (velocity vector $\boldsymbol{V}_{ISN\infty}$), and temperature [1, 2, 3, 4, 5], in agreement with Ulysses GAS [6, 7, 8] (**Fig. 1**). The interstellar magnetic field $\boldsymbol{B}_{IS}$ is deduced from the IBEX ribbon, consistent with the heliospheric asymmetry and TeV cosmic ray anisotropy [9]. The two vectors define the $\boldsymbol{B}_{IS}$- $\boldsymbol{V}_{ISN\infty}$ plane, which determines the shape of, and the flow deflection in, the outer heliosheath [10, 11]. An independent determination of $\lambda_{ISN\infty}$ will tighten $\boldsymbol{V}_{ISN\infty}$, and obtaining $\lambda_{ISN\infty}$ over an extended time will resolve a current debate on possible temporal variations [12, 13, 14].

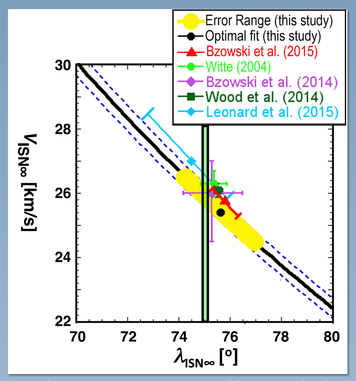

FIGURE 1: Relationship between $V_{ISN\infty}$ and $\lambda_{ISN\infty}$ according to the IBEX parameter tube based on various IBEX analyses in comparison with Ulysses results (adapted from [5]). Also shown with a vertical bar is how an independent measurement of $\lambda_{ISN\infty}$ will constrain the ISN flow vector. The effect of a precise independent determination of the ISN flow longitude $\lambda_{ISN\infty}$ on the knowledge of the ISN flow parameters is indicated by the green vertical bar.

Pickup Ion Cut-Off Modeling

- **Robust method to obtain $\lambda_{ISN\infty}$:** Pickup ion (PUI) cut-off speed (high-energy edge of the PUI distribution) is a function of the ratio V_r/V_{SW} (radial ISN flow component and solar wind speed) [16]

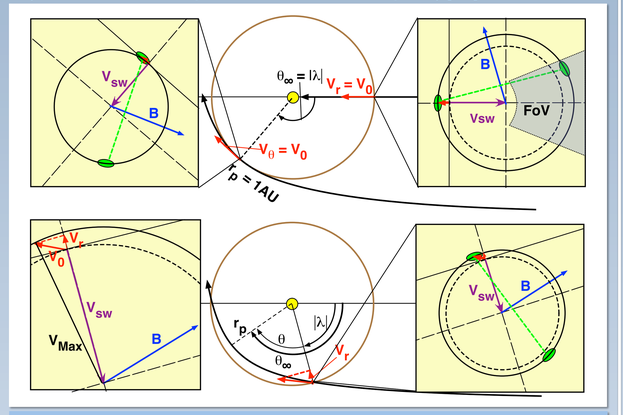

FIGURE 2: Schematic view of ISN trajectories with varying angular momenta and resulting radial V_r and tangential V_θ velocity components at various longitudes λ from upwind [16].

Top: Exactly upwind (right) and where the ISN flow is tangential to the Earth's orbit (left).

Bottom: Arbitrary location between the former two. The insets on the upper left and right and the lower right show a cut through the resulting PUI velocity distribution in the $\boldsymbol{V}_{SW}$ and $\boldsymbol{B}_{IMF}$ (interplanetary magnetic field) plane in the solar wind frame. Shown is the initial torus distribution upon injection at the combined solar wind and ISN flow velocity for $\boldsymbol{B}_{IMF}$ so that the torus is fully in the STEREO PLASTIC FOV (top right). The dashed circle indicates the edge of the PUI distribution for $V_r = 0$. The blow-up in the lower left shows how the velocity components add up to the maximum PUI speed V_{Max}.

- **Radial ISN flow $v_r = V_r/V_E$** (normalized to Earth's speed) varies with λ [16]

$$v_r^2 = 2 + v_{ISN\infty}^2 - (1-\cos\lambda) - \left\{ v_{ISN\infty}^4 \sin^2\lambda + v_{ISN\infty} \sin|\lambda| \left[v_{ISN\infty}^2 \sin^2\lambda + 4(1-\cos\lambda) \right]^{1/2} \right\} / 2 \quad (1)$$

- **v_r is at maximum exactly upwind** ($\lambda_{Obs} = \lambda_{ISN\infty} + 180°$ or $\lambda = 0$)
- **v_r decreases symmetrically with $|\lambda|$**
- **$v_r = 0$: ISN bulk flow reaches 1AU perihelion at λ_0** [17] $\cos\lambda_0 = -(1 + v_{ISN\infty}^2)^{-1}$ (see **Fig. 2**)

PUI Cut-Off with STEREO PLASTIC & ACE SWICS

As shown in **Fig. 2**, the cut-off speed in the solar wind frame to a good approximation is given by $V_{SW} + V_r$. Normalized to V_{SW} it is then:

$$w'_{CutOff} = (V_{SW} + V_r) / V_{SW} \quad (2)$$

PUI distributions are gyrotropic and mostly scatter in pitch angle. As shown recently [18], they largely maintain their initial torus distribution with some scattering, which introduces a Φ_B dependent w_{CutOff} bias in the rest frame. **Fig. 3** shows a distribution obtained with PLASTIC after transformation into the solar wind frame (w') in the $\boldsymbol{B}_{IMF}$-$\boldsymbol{V}_{SW}$ plane. Accumulation along shells in constant w' produces a cut-off that does not depend on the $\boldsymbol{B}_{IMF}$ angle.

- **Cut-off speed only minimally affected by PUI transport effects**
  Produced by newborn ions and not altered by pitch angle scattering

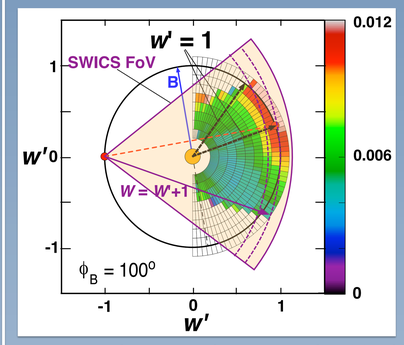

FIGURE 3: PUI distribution obtained with STEREO PLASTIC in the plane that contains the solar wind and interplanetary magnetic field for $\phi_B = 100°$, in the solar wind frame and subdivided by the dimensionless PUI speed w' and angle ϕ (adapted from [18]). Also shown is the full spin-integrated ACE SWICS FOV along with the subdivision in PUI speed w in the spacecraft frame.

- **SWICS and PLASTIC phase space densities (PSD) and PLASTIC normalized counts in w' across the cut-off** are shown in **Fig. 4** (with data used for PLASTIC and SWICS cross-calibration [19])

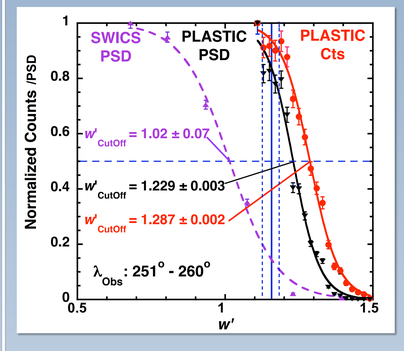

Figure 4: PUI spectra near the cut-off in the upwind direction (251° < λ_{Obs} < 260°) and statistical uncertainties. The PLASTIC spectra (normalized counts in red and normalized PSD in black) are accumulated on circles of constant w' (black circle in **Fig. 3**) and the SWICS spectrum on constant w (magenta arcs in **Fig. 3**). Also shown are fits to a hyperbolic tangent, the inflection points (horizontal dashed line), and the model value of w'_{CutOff} (solid blue line) for λ_{Obs} = 255° with the standard deviation of the observed cut-off values (dashed blue lines).

The cut-off values obtained with PLASTIC are noticeably higher than model values computed with equations (1) and (2)

- **Model describes ISN bulk flow** (center of the torus distribution in **Fig. 3**)
  - Finite ISN temperature broadens torus → Higher Cut-off
  - Sensor energy resolution broadens torus → Higher Cut-off
  - Normalized counts: Energy flux density ~ PSD x w^4 → Higher Cut-off
- **Accumulation over entire SWICS FOV in spacecraft frame** → Lower cut-off as evident in **Fig. 3**.
- **Same accumulation procedure for PLASTIC** → Also lower cut-off as seen in SWICS and PLASTIC cross-calibration spectra [19]
- **Even small variation** in $\boldsymbol{B}_{IMF}$ angle Φ_B **alters the observed cut-off values**
  When taken with ACE SWICS as shown here
  → Future subdivision by spin angle sectors
  → Forward modeling of PSD distribution for observed $\boldsymbol{V}_{SW}$, $\boldsymbol{B}_{IMF}$, etc.
  will minimize these variations
- **In the following:**
  - Use PLASTIC normalized count data (observed quantities) to test method
  - Illustrate how individual years with PLASTIC affect results
  - Illustrate how untransformed data with SWICS affect results

PUI Cut-Off Variation with Ecliptic Longitude

- **Use of PUI Cut-Off obtained as shown in Fig. 4 as a function of λ_{Obs}**

FIGURE 5: PUI Cut-off as a function of observer longitude λ_{Obs}, obtained from a fit of the respective PUI distributions in 1° increments to a hyperbolic tangent with fit uncertainties, as illustrated in **Fig. 4**. Normalized counts are used for PLASTIC and PSD for SWICS.

Top: STEREO PLASTIC observations of the PUI cut-off in the solar wind frame (w'), constrained to V_{SW} < 450 km/s and $\boldsymbol{B}_{IMF}$ so that the torus is completely within the PLASTIC FOV, combining 2007-2014.

Center: STEREO PLASTIC observations from 2007.

Bottom: ACE SWICS observations from 2007, constrained in $\boldsymbol{B}_{IMF}$ so that the angle between $\boldsymbol{B}_{IMF}$ and the solar wind is >75°. Compared with STEREO PLASTIC, the ACE SWICS data are not transformed into the solar wind frame and thus still contain a considerable dependence on the $\boldsymbol{B}_{IMF}$ direction, as illustrated in **Fig. 3**. We simply took $w'_{CutOff} = w_{CutOff} - 1$.
Also shown is the PUI cut-off model curve (in blue, Eq. 1 & 2) assuming $\lambda_{ISN\infty}$ = 75°.
To account for the effects discussed in **Fig. 3**, the predicted w'_{CutOff} values are shifted by
$\Delta w'$ = +0.15 for PLASTIC and
$\Delta w'$ = -0.2 for SWICS to obtain the best fit.
The green arrows and yellow highlight boxes make a connection to **Fig. 6** and are described below.

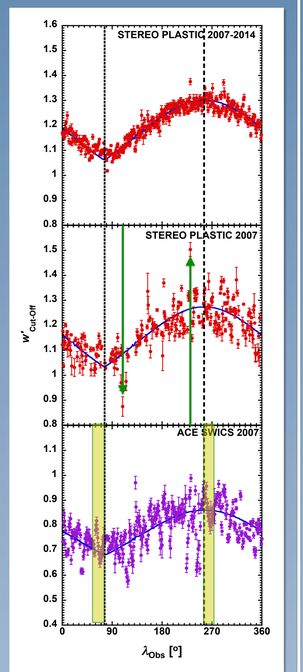

As seen in **Fig. 5**, the scatter of the cut-off values about the best fit model curve increases when using only one year (2007) of PLASTIC data and SWICS data, and for SWICS systematic swings appear (two highlighted). To explore the latter, we show the variation of V_{SW} for the two 2007 data sets with the standard deviation of the individual points in **Fig. 6**.

FIGURE 6: Solar wind speed as a function of ecliptic longitude, including its standard deviation for 1° samples over the year 2007.

Top: Averaged for the STEREO PLASTIC PUI data selection:
- V_{SW} < 450 km/s
- Only times taken with IMF direction so that the PUI torus distribution is completely within the PLASTIC FOV
- The vertical green lines point to the start of a gap due to the V_{SW} restriction. They coincide in λ_{Obs} with the green arrows in **Fig. 5**, which point to PUI Cut-Off outliers.

Bottom: Averaged for the ACE SWICS PUI data selection:
- Only times taken with IMF direction so that $\theta_{BVsw} > 75°$
- The highlight boxes indicate large V_{SW} swings, which coincide with large systematic variations in the cut-off values in **Fig. 5**.

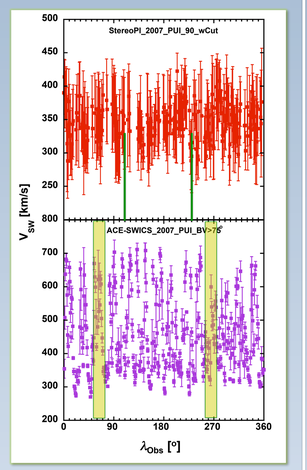

- **With no restrictions in V_{SW} for SWICS, V_{SW} in Fig. 6 is almost bi-modal**
  → Partially reflected in cut-off values in **Fig. 5**
- **Huge V_{SW} swings coincide with cut-off swings** (highlighted in **Fig. 5&6**)
- **PLASTIC shows less systematic variations, but some visible outliers**
  → Coincide with transitions to cut-out high V_{SW} (vertical green lines)
- **V_{SW} variations often connected to solar wind compressions**
  → Such systematic effects must be studied in detail
- **Systematic variations occur stochastically across years**
  → Influence can be mitigated in multi-year/longitude combinations [20]

Preliminary ISN Flow Longitude Determination

- **Pearson correlation between cut-off values & mirror image about λ_M**

FIGURE 7: Pearson correlation coefficient between the measured cut-off values w'_{CutOff} from **Fig. 5** as a function of observer longitude and the same values, mirrored about the longitude λ_M, which is incremented in 1° steps for ±90° about λ_{Upwind}. Also shown is the best-fit curve to a cosine function, along with the fit values and fit uncertainty for λ_{Upwind} and $\lambda_{ISN\infty}$. The vertical dashed line indicates the upwind direction based on the entire STEREO PLASTIC data set.

Top: STEREO PLASTIC observations from 2007 through 2014.

Center: STEREO PLASTIC observations from 2007.

Bottom: ACE SWICS observations from 2007.

The data selection is identical to the one used for the cut-off values as a function of observer longitude shown in **Fig. 5**.

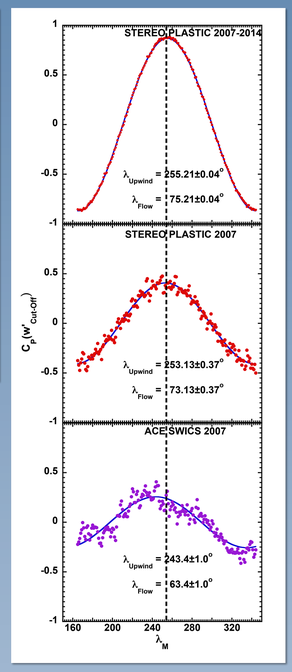

Results & Outlook

- **ISN Flow Direction from PLASTIC Data 2007-2014: $\lambda_{ISN\infty}$ = 75.21±0.04°**
  - Consistent with other observations & very small statistical uncertainty
    → **So far only proof of concept**: Systematic effects must be studied
    E.g.: V_{SW}, compressions, rarefactions, $\boldsymbol{B}_{IMF}$, wave power
  - **Promises very tight result for $\lambda_{ISN\infty}$ ←→ Synergism with IBEX!**
- **Systematic Effects evident in 1-Year Data (2007 PLASTIC & SWICS)**
  - Visible as deviations from STEREO PLASTIC multi-year result
    → Restriction of V_{SW} & transformation reduces effect from ≈10° to ≈2°
  - Systematics randomized across years & longitude (STEREO A & B, ACE)
    Already successfully applied to Focusing Cone & Crescent [20]
- **PUI Cut-Off Method uses Newborn Ions → Transport Effects Minimized**
  - Only pitch angle scattering → No effect in solar wind frame
- **18+ Year Data Sets (STEREO, ACE & SOHO) for He, O & Ne**
  → Will provide constraints on potential time variations in ISN Flow
  → Will compare effects of Secondary ISN Component on results and determine Secondary Flow direction for O

References

1. M. Bzowski et al. *Astrophys. J. Supp.* **220**:28 (2015).
2. T. Leonard et al., *Astrophys. J.* **804**:42 (2015).
3. D. J. McComas et al., *Astrophys. J. Supp*. **220**:22 (2015).
3. E. Möbius et al., *Astrophys. J. Supp.* **220**:24 (2015).
4. N.A. Schwadron et al., *Astrophys. J. Supp.* **220**:25 (2015).
6. M. Witte, *Astron. & Astrophys.* **426**, 835 (2004).
7. M. Bzowski et al., *Astron. & Astrophys.* **569**, A8 (2014).
8. B. Wood, H.-R. Mueller & M. Witte, *Astrophys. J.* **801**:62 (2015).
9. N.A. Schwadron et al., *Science* **343**, 988 (2014).
10. R. Lallement et al., *Science* **307**, 1447 (2005).
11. V. Izmodenov, D. Alexashov & A. Myasnikov, *Astron. & Astrophys*. **437**, L35 (2005).
12. P.C. Frisch et al., *Science* **341**, 1080 (2013).
13. P.C. Frisch et al., *Astrophys. J.* **801**:61 (2015).
14. R. Lallement & J.-L. Bertaux, *Astron. & Astrophys*. **565**, A41 (2014).
15. E. Möbius et al., *Geophys. Res. Lett*. **26**, 3181 (1999).
16. E. Möbius, M. A. Lee & C. Drews, *Astrophys. J.*, **815**:20 (2015).
17. M. A. Lee, E. Möbius & T. Leonard, *Astrophys. J. Supp*. **220**:23 (2015).
18. C. Drews et al. *Astron. & Astrophys*. **575**, 97 (2015).
19. E. Möbius et al., *AIP Conf. Proc*. **1302**, 37 (2010).
20. C. Drews et al., *J. Geophys. Res*. **117**, 9106 (2012).